13th International Symposium on Turbulence and Shear Flow Phenomena (TSFP13)
Montreal, Canada, June 25–28, 2024

ADVANCING WALL-MODELLED LARGE-EDDY SIMULATIONS: A LAGRANGIAN RELAXATION APPROACH FOR ROUGH SURFACES

Teresa Salomone
Dept. of Mechanical and Materials Engineering
Queen's University
Kingston, ON, K7L 3N6, Canada
teresa.salomone@queensu.ca

Charles Meneveau
Dept. of Mechanical Engineering
Johns Hopkins University
3400 N. Charles Street, Baltimore, MD 21218, USA
meneveau@jhu.edu

Giuliano De Stefano
Engineering Dept.
University of Campania Luigi Vanvitelli
81031 Aversa, Italy
giuliano.destefano@unicampania.it

Ugo Piomelli
Dept. of Mechanical and Materials Engineering
Queen's University
Kingston, ON, K7L 3N6, Canada
ugo@queensu.ca

ABSTRACT

Heterogeneous surface-roughness is present in many applications in engineering and natural sciences, and numerical simulations are a fundamental tool to investigate the fluid flow in this type of surface conditions. Wall-Modelled Large-Eddy Simulations (WMLES) are particularly effective in decreasing the computational cost of the simulations at the expense of additional modelling. In this work, the "generalized Moody diagram" model [Meneveau, J. Turbul. 21(11):650–673 , 2020], with inclusion of mild pressure gradients, and the "Lagrangian Relaxation-Towards-Equilibrium" (LaRTE) model [Fowler et al., J. Fluid Mech. 934:A44, 2022] were used to simulate the flow over roughness strips placed normal to the mean flow. A new formulation of the LaRTE model for rough walls is proposed that allows the model to switch seamlessly between smooth-wall behaviour and transitionally or fully-rough flow conditions. Simulations with the standard log-law Equilibrium Wall-Model (EQWM) were also performed and used as a comparison, and the present numerical results were validated against experimental data. Simulations on smooth and homogeneous rough-walls show that the new formulation of the LaRTE model effectively allows the prediction of the flow in both smooth and fully-rough regimes. In the heterogeneous rough wall case, the LaRTE model improves the prediction of the skin-friction coefficient, especially on the rough strips, and the turbulent non-equilibrium portion of the model is required to represent accurately the return to equilibrium on the smooth strip.

INTRODUCTION

Roughness is often present in many engineering and natural science fluid dynamics applications. Its impact manifests as: heightened drag (Nikuradse (1933)), disruption of the production mechanism of turbulent kinetic energy within the near-wall region (Raupach *et al.* (1991); Finnigan (2000)), and attenuation of the anisotropy of Reynolds stresses (Shafi & Antonia (1995)). When roughness is distributed heterogeneously, additional effects emerge due to the different wall-boundary condition at which the flow is subjected.

An example of roughness heterogeneity manifests in the form of alternating rough-patches characterized by varying heights, positioned orthogonal to the mean flow. This configuration is commonly found in atmospheric boundary layers (Cheng & Castro (2002); Chamorro & Porté-Agel (2009)), and meteorological flows (Garratt (1990)). Experimental investigations into this particular configuration (Antonia & Luxton (1971, 1972); Li *et al.* (2019)) revealed the formation of an internal boundary layer downstream of the surface transition. This layer segregates the region proximal to the wall, influenced by the new surface condition, from the more distant region, which retains characteristics related to the upstream surface condition.

Numerical simulations, together with experiments, represent an essential tool to study the flow in heterogeneous rough-walls configurations, but Direct Numerical Simulation (DNS) and Wall-Resolved Large-Eddy Simulation (WRLES) are limited to low Reynolds-number flows (Jiménez (2004)). Modelling the near-wall region is the only way numerical simulations of high Reynolds-number flows over rough walls can be performed at a reasonable computational cost (e.g., Salomone *et al.* (2023)).

Several wall models for Large-Eddy Simulation (LES) have been developed during the past years, with some of them reviewed by Larsson *et al.* (2016). The most common type of wall models are those named as "wall-stress models", where the inner-layer is replaced by a single quantity, namely the wall-shear stress τ_w, used as a wall-boundary condition for the LES field. In this context, the classical log-law Equilibrium Wall-Model (EQWM) remains the most commonly used, but alternative wall-stress models have been recently proposed, such as the "generalized Moody diagram" of Meneveau (Meneveau (2020)) and the "Lagrangian Relaxation-Towards-Equilibrium" (LaRTE) proposed by Fowler *et al.* (2022).

The generalized Moody diagram, here named as GMD model, is constructed by various fitting functions to the solution of the one-dimensional Reynolds Averaged Navier–Stokes (RANS) equation in its simple boundary-layer approximation. The fitting functions allow the calculation of the wall-shear stress not only in equilibrium conditions, but also in the presence of mild

and strong pressure gradients, as well as surface roughness.
The LaRTE model, which lies in the integral wall-models category, was developed as an extension of the modelling procedure proposed by Yang *et al.* (2015), where a Partial Differential Equation (PDE) for the friction velocity was found through the integration of the RANS equations for the wall-parallel velocity. The model was originally developed for smooth walls, while an extension to rough walls is proposed in this work. The novel approach allows the recovery of the smooth-wall behavior seamlessly, and can also include transitionally-rough cases.
Both these models were used to simulate the flow in a heterogeneous-roughness configuration given by alternating rough and smooth strips oriented normal to the mean flow. For comparison, the simulation employing the standard EQWM was also conducted. The present numerical simulations were performed at flow conditions and domain characteristics comparable to the experimental work of Li *et al.* (2019). Additionally, comparisons were made between the simulation results and the experimental data of Antonia & Luxton (1971), to further assess the accuracy of the proposed wall-models in predicting the re-adjustment of flow variables after a surface transition.

METHODOLOGY

The LES governing equations for incompressible flow are:

$$\frac{\partial \hat{u}_i}{\partial x_i}=0;\frac{\partial \hat{u}_i}{\partial t}+\frac{\partial}{\partial x_j}(\hat{u}_i\hat{u}_j)=-\frac{\partial \hat{p}}{\partial x_i}+\nu\nabla^2\hat{u}_i-\frac{\partial \tau_{ij}}{\partial x_j}, \quad (1)$$

where the hat operator represents the LES spatial filtering. In these equations $\hat{u}_i$ is the filtered velocity in the three spatial directions: $x_1 \equiv x$ streamwise, $x_2 \equiv y$ wall normal, and $x_3 \equiv z$ spanwise, associated with u, v, w velocity components, respectively; $\hat{p} = P/\rho$ stands for the modified pressure, ν is the constant kinematic viscosity, and $\tau_{ij} = \widehat{u_i u}_j - \hat{u}_i\hat{u}_j$ the residual (unresolved) stresses. The latter are modelled through an eddy-viscosity assumption for the deviatoric part of the stress tensor:

$$\tau^d_{ij} \equiv \tau_{ij} - \frac{1}{3}\delta_{ij}\tau_{kk} = -2\nu_T \hat{S}_{ij}\ , \quad (2)$$

where

$$\hat{S}_{ij} = \frac{1}{2}\left(\frac{\partial \hat{u}_i}{\partial x_j}+\frac{\partial \hat{u}_j}{\partial x_i}\right) \quad (3)$$

is the resolved strain-rate tensor. Here, the model proposed by Vreman (2004) is used for the sub-filter stresses, with the standard value of the model constant. The governing equations are advanced in time with a fractional step method. The Crank-Nicolson time advancement was used for the wall-normal diffusion, and a third-order Runge-Kutta scheme was used for the remaining terms. Conservative second-order finite differences on a staggered grid were used for the spatial discretization. Periodic boundary conditions are applied in the streamwise and spanwise directions, and a symmetry condition is applied at the top boundary. The bottom-wall boundary condition varies depending on the wall model that is used. The wall-model interface is fixed at a distance from the wall $\Delta/\delta = 0.05$, allowing three grid points to be located below the interface, following the recommendations of Kawai & Larsson (2012).

Wall Models

The wall region was addressed using wall models, which relate the wall stress to the velocity in the outer region. The use of this models is standard in LES of high-Reynolds number flows, since the grid requirements set by the inner layer make wall-resolved LES inaccessible.

One of the most commonly used models of this type is the standard log-law model, in which the wall stress is derived by numerically solving the logarithmic law-of-the-wall for smooth and rough surfaces:

$$u^+ = \kappa^{-1}\log(y^+) + B \quad (4)$$

$$u^+ = \kappa^{-1}\log(y/k_s) + 8.5, \quad (5)$$

where the symbol $+$ is used to express inner-units normalization, $\kappa = 0.4$, and $B = 5$, while k_s is the equivalent sand-grain roughness height, representing a measure of the drag induced by the roughness. Equation (4) must be solved with iterative methods, whereas (5) can be explicitly solved once k_s has been fixed.
In the GMD model, the streamwise RANS momentum equation in its boundary-layer approximation is integrated and fitting functions are developed for its solution. The equation is integrated in a dimensionless framework where two Reynolds numbers and the normalized pressure gradient are defined as:

$$Re_\Delta = \frac{|U_{LES}|\Delta}{\nu},\ Re^{ufs}_{\tau\Delta} = \frac{u_\tau\Delta}{\nu},\ \psi_p = \frac{1}{\rho}(\partial_j P)\frac{\Delta^3}{\nu^2}. \quad (6)$$

Here, Δ is the location of the wall-model interface above the wall, $|U_{LES}|$ is the magnitude of the LES velocity at the wall-model interface $U_{i,LES} = \hat{u}_i(x,\Delta,z,t)$, and u_τ is the friction velocity. Also, Re_Δ is the input parameter of the wall model and $Re^{ufs}_{\tau\Delta}$ is the fitted solution from which the friction velocity is calculated. The fit for $Re^{ufs}_{\tau\Delta}$ can be characterized as a fully equilibrium model, which does not require numerical integrations or iterations for solving Equation (4). Roughness and pressure gradient effects can be included in the modelling procedure. The interested readers are referred to the original manuscript for further details (Meneveau (2020)).

In the LaRTE model, a PDE for the friction velocity is found through the integration of the RANS equation for the wall-parallel momentum components. The assumption is that from the wall surface up to the wall-model interface, an equilibrium layer exists where the wall-parallel mean velocity, $\bar{\mathbf{u}} = \overline{u}\hat{\mathbf{\imath}} + \overline{w}\hat{\mathbf{k}}$, can be expressed as:

$$\overline{u}_i(x,y,z,t)\rangle = u_{\tau i}(x,z,t) f(y^+) \quad (7)$$

where $(\bar{\cdot})$ represents time or spatial average, and $u_{\tau i}$ is the friction-velocity vector. $f(y^+)$ is an inner-layer similarity function that represents the mean velocity below the wall-model interface. Equation (7) is substituted into the momentum equation for the wall-parallel velocity, consistently with the boundary-layer approximations (Fowler *et al.* (2022)), and then integrated to find an evolution equation for $u_{\tau i}$:

$$\frac{\partial u_{\tau i}}{\partial t} + V_{\tau j}\partial_j(u_{\tau i}) = \frac{1}{T_s}\left[\frac{1}{u_\tau}\left(-\frac{\Delta}{\rho}\partial_i \overline{p}' + \overline{\tau}_{\Delta i}\right) - u_{\tau i}\right] + u_\tau \frac{\partial s_i}{\partial t}\frac{\delta^*_\Delta}{\Delta} + \mathscr{F}_{1i}\frac{\theta_\Delta}{\Delta}. \quad (8)$$

In this equation the left-hand-side is the Lagrangian time derivative, in which the convection velocity is

$$V_{\tau i} = (1 - \delta^*_\Delta/\delta - \theta_\Delta/\delta) f(\Delta^+) u_{\tau i}; \tag{9}$$

$T_s = f(\Delta^+)\Delta/u_\tau$ is the relaxation timescale, $\overline{p}'$ is the fluctuating pressure field, $\tau_{\Delta i}$ is the stress at the wall-model interface, s_i is the unit vector in the wall-parallel directions, $\mathscr{F}_{1i}$ is a function that includes the spatial derivatives of the friction-velocity vector, and δ^*_Δ and θ_Δ are the displacement and momentum thicknesses, respectively, defined by using Equation (7) for velocity, and integrating up to Δ. The treatment of the fluctuating pressure is discussed in Fowler *et al.* (2022).
Equation (8) requires a closure for the stress at the wall-model interface $\overline{\tau}_{\Delta i}$, which is achieved using the GMD model to relate $\overline{\tau}_{\Delta i}$ to known LES quantities (6). In summary, (8) represents the transition of the quasi-equilibrium friction-velocity vector, $u_{\tau i}$, towards the stress at the interface $\tau_{\Delta i}$ (including the influence of the pressure gradient) over the relaxation timescale T_s. Additional non-equilibrium effects can be introduced separately, as will be discussed momentarily. More details on the LaRTE model formulation can be found in the original work by Fowler *et al.* (2022).

An extension to Equation (8) for rough surfaces, incorporating the definition of the equivalent sand-grain roughness height, k_s, can be derived by modifying the approach outlined in Equation (7). The wall-parallel mean velocity is then rewritten as

$$\overline{u}_i(x,y,z,k_s^+,t) = u_{\tau i}(x,z,t) F(y^+,k_s^+) \tag{10}$$

where $F(y^+,k_s^+) = f(y^+) - f_{NW}(y^+)\Delta U^+(k_s^+)$; As for the smooth case, $f(y^+)$ is a log-law profile that transitions into the linear region, while $f_{NW}(y^+)\Delta U^+(k_s^+)$ accounts for the roughness. The function $F(y^+,k_s^+)$ resulting from this procedure is plotted in Figure 1. When $k_s^+ = 0$, $F(y^+,k_s^+) = f(y^+)$, and the smooth inner-similarity function is recovered. When $k_s^+ > 0$, the velocity profile shifts downward as an effect of the increasing drag. The amount by which the profile is shifted is obtained from the empirical formula (Colebrook (1939)):

$$\Delta U^+ = \kappa^{-1} \log(1 + 0.26 k_s^+) \tag{11}$$

The integration of the wall-parallel RANS momentum equation, using Equation (10) for the wall-parallel velocity, leads to a new equation for the friction-velocity vector that retains all the smooth contributions, but includes additional terms that account for the roughness, specifically:

$$\begin{aligned}
\frac{\partial u_{\tau i}}{\partial t} + V_{\tau j}\partial_j(u_{\tau i}) &= \frac{1}{T_s}\left[\frac{1}{u_\tau}\left(-\frac{\Delta}{\rho}\partial_i \overline{p}' + \overline{\tau}_{\Delta i}\right) - u_{\tau i}\right] \\
&+ u_\tau \frac{\partial s_i}{\partial t}\frac{\delta^*_\Delta}{\Delta} + \mathscr{F}_{1i}\frac{\theta_\Delta}{\Delta} \\
&+ 2\frac{f_\Delta}{F_\Delta}\mathscr{F}_{2i}\left(1 - \frac{\delta^*_{\Delta S}}{\Delta} - \frac{\theta_{\Delta f f_{NW}}}{\Delta}\right) \\
&- 2\frac{f_{NW}(\Delta^+)\Delta U^+}{F_\Delta}\mathscr{F}_{2i}\left(1 - \frac{\delta^*_{\Delta NW}}{\Delta} - \frac{\theta_{\Delta NW}}{\Delta}\right) \\
&- \mathscr{F}_{2i}\left(1 - \frac{\delta^*_{\Delta NW}}{\Delta}\right) \\
&+ s_i \frac{\partial u_\tau}{\partial t}\frac{k_s^+(\Delta U^+)' f_{NW}(\Delta^+)}{F_\Delta}\left(1 - \frac{\delta^*_{\Delta NW}}{\Delta}\right).
\end{aligned} \tag{12}$$

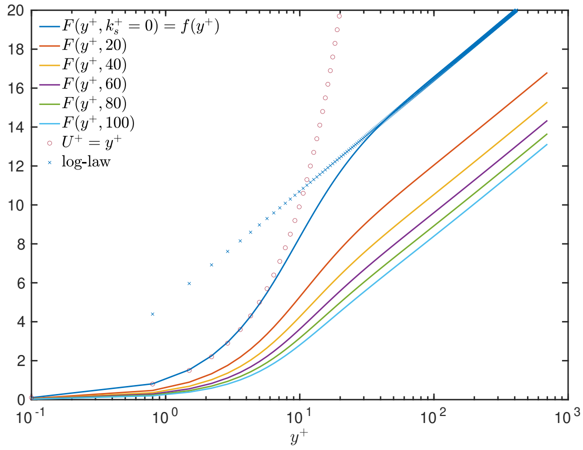

Figure 1. Inner-similarity function in the LaRTE model formulation for rough walls.

The first three terms on the right-hand side of Equation (12) are also present in the smooth formulation (8), whereas additional terms appear from the roughness extension. The displacement and momentum thicknesses, δ^*_Δ and θ_Δ, are evaluated using the new similarity function $F(y^+,k_s^+)$. The terms $\delta^*_{\Delta S}$ and $\delta^*_{\Delta NW}$ are determined using the smooth function $f(y^+)$ and the near-wall function $f_{NW}(y^+)$, respectively. The momentum thickness $\theta_{\Delta f f_{NW}}$ involves the product $f(y^+) f_{NW}(y^+)$, while $\theta_{\Delta NW}$ utilizes $f_{NW}(y^+)$. The term $(\Delta U^+)'$ is the derivative of ΔU^+ with respect to k_s^+. Equation (12) represents a model for the friction-velocity vector, where the roughness is accounted for explicitly.

Surface heterogeneity is included through the spatial derivatives in the function $\mathscr{F}_{2i}$

$$\begin{aligned}
\mathscr{F}_{2i} &= u_{\tau i} u_{\tau j}\,\partial_j k_s^+ \,(\Delta U^+)' f_{NW}(\Delta^+) \\
&= \left(u_{\tau i} u_{\tau j}\frac{\partial k_s}{\partial x_j} u_\tau + u_{\tau i} u_{\tau j}\frac{\partial u_\tau}{\partial x_j} k_s\right)\frac{(\Delta U^+)' f_{NW}(\Delta^+)}{\nu}.
\end{aligned} \tag{13}$$

The definition above involves the derivative of k_s in the spatial directions, making this term directly accountable for flow alterations caused by roughness heterogeneity. Furthermore, when $\Delta U^+ = 0$, i.e. the wall is smooth, the function $\mathscr{F}_{2i}$ and the last term in Equation (12) are identically equal to zero, recovering the smooth-wall equation. Note that both Equation (8) and Equation (12) model the quasi-equilibrium part of the wall stress, with the difference that the latter also includes roughness heterogeneity.

Non-equilibrium effects can be added separately. The turbulent non-equilibrium (turbNEq) part of the wall stress is considered (Fowler *et al.* (2023)), relating the LES velocity and the LaRTE solution through the definition of the following turbulent velocity fluctuation:

$$u'_{i\Delta} = U_{i,LES} - u_{\tau i} f(\Delta^+). \tag{14}$$

This additional contribution accounts for velocity differences between the LES field $U_{i,LES}$ and the quasi-equilibrium solution $u_{\tau i} f(\Delta^+)$. The turbulent velocity fluctuation $u'_{i\Delta}$ can be interpreted as stemming from the presence of large, wall-attached eddies with heights approximately equal to Δ as stated in the attached eddy hypothesis of Townsend (1976). The turbulent non-equilibrium wall-stress is given by

$$\tau'_{wi} = \frac{u_\tau u'_{i\Delta}}{l_s^+} \tag{15}$$

where u_τ is the magnitude of the friction-velocity vector and $l_s^+ = 12$ is the height of the assumed laminar Stokes layer, where a linear shear layer exists connecting the velocity profile to the no-slip boundary condition at the wall. In conclusion, the total wall-shear stress in the LaRTE model is evaluated as the superposition of the quasi-equilibrium and the turbulent non-equilibrium components:

$$\tau_{wi} = u_\tau u_{\tau i} + \tau'_{wi}, \tag{16}$$

which are given by Equation (12) and Equation (15), respectively. The new extension of the LaRTE model to rough walls is named as LaRTE-RW in the following sections. Equation (12) is discretized using a forward Euler method (Fowler *et al.* (2022)).

RESULTS

To test the new LaRTE-RW model, WMLES are performed for statistically stationary open-channel flow, for both homogeneous and heterogeneous roughness. Flow conditions and grid resolution were kept the same among the different simulations so that any difference in the simulations' results must be attributed to the wall model.

Homogeneous roughness

Homogeneous-roughness simulations employ a domain size of $L_x \times L_y \times L_z$ = $6.4\delta \times \delta \times 3.2\delta$, and a uniform grid of $192 \times 60 \times 94$ points. In both GMD and LaRTE-RW models, the input velocity $|U_{LES}|$ and the pressure gradient ψ_p are temporally filtered with a single-sided exponential filter (Yang *et al.* (2017)). The log-law model, on the other hand, uses the instantaneous value of the velocity at the wall-model interface. The equivalent sand-grain roughness height is $k_s^+ \simeq 130$; calculations with a smooth wall are also performed, to compare with the data of Lee & Moser (2015).

The mean-velocity profile in inner units is shown in Figure 2. In equilibrium conditions, LaRTE-RW and GMD models are expected to be equivalent and, in fact, no major differences can be observed. All the velocity profiles adhere closely to the smooth log-law solution, represented by the solid black line. Comparison with DNS data from Lee and Moser (2015) reveals similarities between the smooth-wall results, except for a minor underestimation of the friction velocity. This discrepancy is also discussed in Fowler *et al.* (2022) and can be attributed to various numerical details, such as grid resolution, subfilter-scale model, etc. (Wang *et al.* (2020)), rather then to the wall models themselves.

Moving on to the case of a homogeneous but rough surface, once again, all velocity profiles exhibit a log-law region. Equation (12) in the LaRTE-RW model switches between the smooth and the fully-rough regimes without the need of additional modelling. The measured roughness function is $\Delta U^+ \simeq 8.5$, consistent with the Colebrook formula and is shown in the inset of Figure 2. Note that the Colebrook formula is built into the model, so this conclusion is only a verification of the consistency and implementation of the model, and not a model prediction.

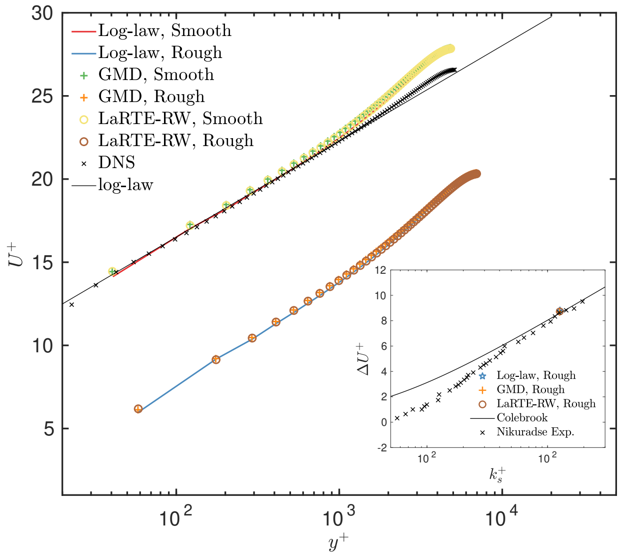

Figure 2. Mean-velocity profile in inner units for homogeneous smooth and rough surface, and (inset) measured roughness function .

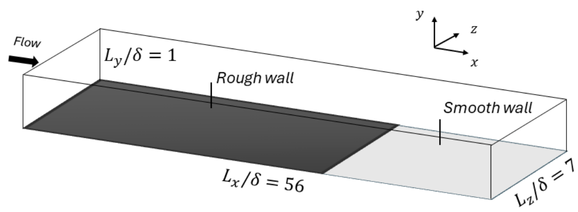

Figure 3. Sketch of the computational domain for heterogeneous-wall simulations (not to scale).

Heterogeneous roughness

Following the models' validation for homogeneous roughness, heterogeneous-roughness simulations were performed. The computational domain is $L_x \times L_y \times L_z$ = $56\delta \times \delta \times 7\delta$, where the rough strip of length L_r occupies 66% of the domain. This geometry is representative of the experimental setup of Li *et al.* (2019), and is shown in Figure 3. Following the notation used in Li *et al.* (2019), the transition location is indicated by x_0, and $\widehat{x} = x - x_0$ is used as the relative streamwise position. In this case, the numerical grid employs $1792 \times 60 \times 224$ points.

The skin-friction coefficient obtained with the different methodologies is shown in Figure 4. The log-law and GMD models closely predict the recovery to equilibrium conditions of the skin-friction coefficient. The GMD model predicts a higher C_f, initially, along the rough strip, due to the mild pressure gradient influence on the model. Overall, there is good agreement with the experimental data, particularly on the smooth strip.

The LaRTE-RW model predicts the discontinuities at the roughness transitions, which would not be shown using Equation (8) alone, as it lacks information about the surface conditions. The recovery of the skin-friction coefficient is improved on the rough strip compared to the log-law and GMD models, highlighting the importance of the terms in (13) that account for the spatial variation of the roughness. The LaRTE-RW model by itself predicts a slower recovery on the smooth strip due to the relaxation timescale T_s, which introduces a delay in approaching the wall stress to the shear-stress at the wall-

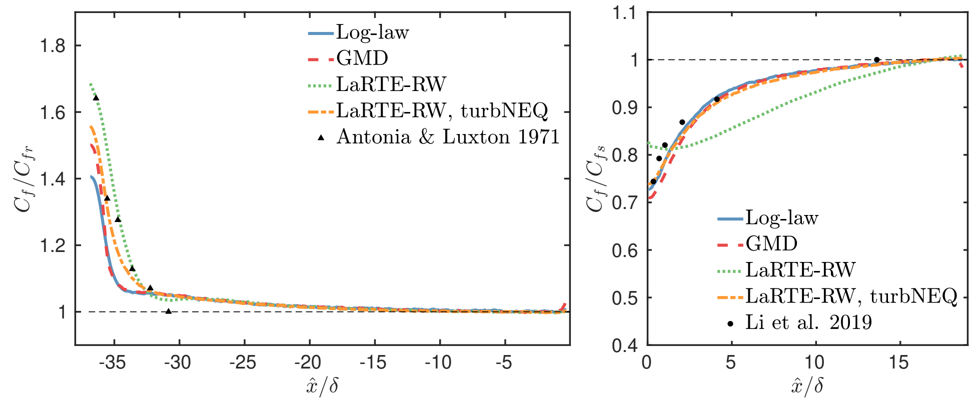

Figure 4. Normalized skin-friction coefficient on the rough strip (left) and smooth strip (right).

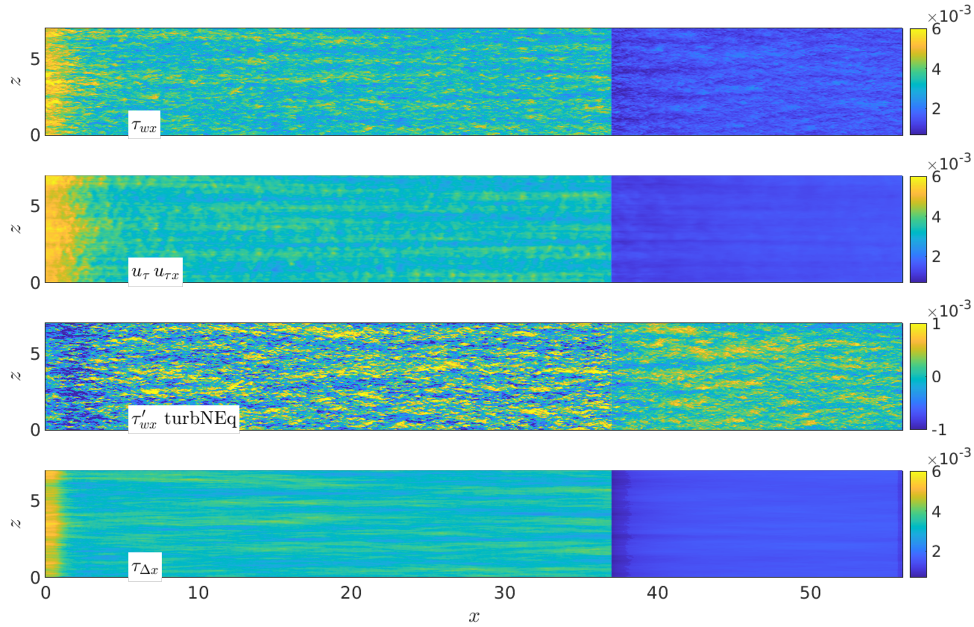

Figure 5. Instantaneous contours of the wall-stress (top three graphs) and the stress at the wall-model interface (bottom graph) with LaRTE-RW model for the streamwise component.

model interface. This phenomenon can be mitigated by incorporating the turbulent non-equilibrium component τ'_{wi}. This additional contribution re-establishes the correlation between stress at the wall and stress at the interface, recovering the skin-friction development of the log-law and GMD models. The C_f recovery is not significantly altered on the rough strip when the turbulent non-equilibrium portion is active, but it slightly diverges from the experimental data. Nevertheless, it is worth noting that the turbulent non-equilibrium portion is based on the existence of a wall-layer that is absent for rough walls. Furthermore, the experimental data of Antonia & Luxton (1971) were collected under different flow conditions than the present numerical simulations, posing challenges in determining whether the turbulent non-equilibrium component provides advantages on the rough strip.

The difference between the LaRTE-RW model and the more traditional log-law and GMD models is that the stress at the wall (computed by solving Equation (12)) differs from the stress at the interface (GMD solution). The instantaneous contour of the different contributions to the stress in the LaRTE-RW model is shown in Figure 5 for the streamwise component. The total wall-stress τ_{wx} is the sum of the LaRTE-RW wall-stress $u_\tau u_{\tau x}$ and the turbulent non-equilibrium portion τ'_{wx}. The LaRTE-RW component is smoother compared to the total wall-stress as a consequence, presumably, of the relaxation time-scale T_s. The fluctuations are re-introduced in the total stress by the turbulent non-equilibrium portion. It is interesting to notice that, although the τ'_{wx} contribution is much lower than $u_\tau u_{\tau x}$, it affects the flow significantly as shown in Figure 4. The stress at the interface, $\tau_{\Delta x}$, has the smoothest appearance, due to its correlation to the time-averaged velocity field at the interface.

CONCLUSIONS

This paper introduces a new extension of the Lagrangian Relaxation-Towards-Equilibrium (LaRTE) model for rough walls, allowing seamless prediction of flow behavior in both smooth and fully-rough regimes. The study compared the new LaRTE model extension with traditional models, namely the Log-Law Equilibrium Wall-Model (EQWM) and the Generalized Moody Diagram (GMD) model. Simulations were conducted for both homogeneous and heterogeneous surface conditions.

In homogeneous-roughness simulations, which provide a check on the implementation of the model, the LaRTE-RW model extension predicts the flow behaviour correctly, closely following the log-law behavior expected for smooth walls and transitioning to rough-wall behavior seamlessly.

In heterogeneous-surface simulations, the prediction of the skin-friction coefficient by GMD and log-law models match, as anticipated. However, the GMD model yields a more pronounced increase at the initial part of the rough strip. This discrepancy can be ascribed to the inclusion of mild-pressure gradients in the model, which are most significant at transition locations. the LaRTE-RW model extension accurately predicts discontinuities at roughness transitions and improves the recovery of the skin-friction coefficient on rough strips, compared to traditional models. A slower recovery is observed on smooth strips, due to the relaxation time-scale introduced by the LaRTE model, but this behaviour can be mitigated by incorporating the turbulent non-equilibrium portion into the wall stress. The proposed roughness extension supplied with the turbulent non-equilibrium part is proven to perform better than standard wall models in predicting the flow in this particular configuration.

However, while the LaRTE-RW model extension enhances prediction accuracy on rough strips, further tests are required in different flow conditions. Additionally, considerations regarding the existence of a wall-layer for rough walls and the influence of experimental conditions on numerical simulations are highlighted as areas for future research.

Acknowledgment

The authors acknowledge the computational support by CINECA under the ISCRA initiative (Project HP10BSBCBZ) and by the Digital Research Alliance of Canada. U.P. acknowledges the financial support from the Natural Sciences and Engineering Research Council (NSERC) of Canada under the Discovery Grant program. C.M. acknowledges the support from the Office of Naval Research, grant N00014-23-1-2185.

REFERENCES

Antonia, R. A. & Luxton, R. E. 1971 The response of a turbulent boundary layer to a step change in surface roughness. Part 1. Smooth to rough. *J. Fluid Mech.* **48** (4), 721–761.

Antonia, R. A. & Luxton, R. E. 1972 The response of a turbulent boundary layer to a step change in surface roughness. Part 2. Rough to smooth. *J. Fluid Mech.* **53** (4), 737–757.

Chamorro, L. P. & Porté-Agel, F. 2009 Velocity and surface shear stress distributions behind a rough-to-smooth surface transition: A simple new model. *Bound.-Layer Meteorol.* **130**, 29–41.

Cheng, H. & Castro, Ian P. 2002 Near-wall flow development after a step change in surface roughness. *Bound.-Layer Meteorol.* **105** (3), 411–432.

Colebrook, C. F. 1939 Turbulent flow in pipes with particular reference to the transition region between smooth- and rough-pipe laws. *J. Inst. Civ. Eng.* **11**, 133–156.

Finnigan, J. 2000 Turbulence in plant canopies. *Annu. Rev. Fluid Mech.* **32** (1), 519–571.

Fowler, M., Zaki, T. A. & Meneveau, C. 2022 A Lagrangian relaxation towards equilibrium wall model for large eddy simulation. *J. Fluid Mech.* **934** (A44), 1–37.

Fowler, M., Zaki, T. A. & Meneveau, C. 2023 A multi-time-scale wall model for large-eddy simulations and applications to non-equilibrium channel flows. *Journal of Fluid Mechanics* **974**, A51.

Garratt, J. R. 1990 The internal boundary layer — a review. *Bound.-Layer Meteorol.* **50**, 171–203.

Jiménez, J. 2004 Turbulent flows over rough walls. *Annu. Rev. Fluid Mech.* **36**, 173–196.

Kawai, Soshi & Larsson, Johan 2012 Wall-modeling in large eddy simulation: length scales, grid resolution, and accuracy. *Phys. Fluids* **24** (1), 015105.

Larsson, J., Kawai, S., Bodart, J. & Bermejo-Moreno, I. 2016 Large eddy simulation with modeled wall-stress: recent progress and future directions. *Mech. Eng. Rev.* **3** (1), 1–23.

Lee, M. & Moser, R. D. 2015 Direct numerica simulation of turbulent channel flow up to $Re_\tau \approx 5,200$. *J. Fluid Mech.* **774**, 395–415.

Li, M., de Silva, C. M., Rouhi, A., Baidya, R., Chung, D., Marusic, I. & Hutchins, N. 2019 Recovery of wall-shear stress to equilibrium flow conditions after a rough-to-smooth step change in turbulent boundary layers. *J. Fluid Mech.* **872**, 472–491.

Meneveau, C. 2020 A note on fitting a generalised Moody diagram for wall modelled large-eddy simulations. *J. Turbul.* **21** (11), 650–673.

Nikuradse, J. 1933 Laws of flow in rough pipes, english translation 1950. *Papers on Mechanical and Physical Subjects* **1** (Tech. Mem. 1292).

Raupach, M. R., Antonia, R. A. & Rajagopalan, S. 1991 Rough-wall boundary layers. *Appl. Mech Rev.* **44** (1), 1–25.

Salomone, T., Piomelli, U. & De Stefano, G. 2023 Wall-modeled and hybrid large-eddy simulations of the flow over roughness strips. *Fluids* **8**, 10.

Shafi, H. S. & Antonia, R. A. 1995 Anisotropy of the Reynolds stresses in a turbulent boundary layer on a rough wall. *Exp. Fluids* **18**, 213–215.

Townsend, A. A. 1976 *Structure of turbulent shear flow*. Cambridge University Press.

Vreman, A. W. 2004 An eddy-viscosity subgrid-scale model for turbulent shear flow: Algebraic theory and applications. *Phys. Fluids* **16** (10), 3670–3681.

Wang, L., Hu, R. & Zheng, X. 2020 A comparative study on the large-scale-resolving capability of wall-modeled large-eddy simulation. *Physics of Fluids* **32** (3).

Yang, Xiang I. A., Park, George Ilhwan & Moin, Parviz 2017 Log-layer mismatch and modeling of the fluctuating wall stress in wall-modeled large-eddy simulations. *Phys. Rev. Fluids* **2**, 104601.

Yang, X. I. A., Sadique, J., Mittal, R. & Meneveau, C. 2015 Integral wall model for large eddy simulations of wall-bounded turbulent flows. *Phys. Fluids* **27** (2), 025112.